# Pulsed Plasma Physical Vapour Deposition Approach Towards the Facile Synthesis of Multilayer and Monolayer Graphene for Anticoagulation Applications

*Rajani K Vijayaraghavan, [1]* Cezar Gaman, [2] Bincy Jose,[3,†] Anthony P McCoy,[4] Tony Cafolla,[4] Patrick J McNally [2] and Stephen Daniels [1]*

[1]National Centre for Plasma Science and Technology, [2]School of Electronic Engineering,

[3]Biomedical Diagnostics Institute, [4]School of Physical Sciences,

Dublin City University, Glasnevin, Dublin 9, Ireland.

[†]Department of histopathology, School of Medicine, Trinity College Dublin.

*Corresponding author.

rajani.vijayaraghavan@dcu.ie

**ABSTRACT**

We demonstrate the growth of multilayer and single layer graphene on copper foil using bipolar pulsed direct current (DC) magnetron sputtering of a graphite target in pure Ar atmosphere. Single layer and few layer graphene films (SG and FLG) are deposited at temperatures ranging from 700-920 °C in less than 30 minutes. We find that the deposition and post-deposition annealing temperatures influence the layer thickness and quality of the graphene films formed. The films were characterized using atomic force microscopy (AFM), scanning electron microscopy (SEM), High resolution transmission electron microscopy (HRTEM), Raman spectroscopy, X-ray photoelectron spectroscopy (XPS) and optical transmission spectroscopy techniques. Based on the above studies, a diffusion controlled mechanism was proposed for the graphene growth. A single step whole blood assay was used to investigate the anticoagulant activity of graphene surfaces. Platelet adhesion, activation and morphological changes on the graphene/glass surfaces compared to bare glass were analysed using fluorescence microscopy and SEM techniques. We have found significant suppression of the platelet adhesion, activation and aggregation on the graphene covered surfaces compared to the bare glass, indicating the anticoagulant activity of the deposited graphene films. Our production technique represents an industrially relevant method for the growth of single and few layer graphene for various applications including the biomedical field.

**KEYWORDS**

Graphene growth, carbon diffusion, sputtered graphene, growth mechanism, anticoagulation, platelet capture

## 1. INTRODUCTION

Graphene is extensively known to be an outstanding material with unique electronic, optical and mechanical properties.[1-3] It remains an exciting area of research due to its potential applications in a wide variety of fields such as high performance sensors, bio imaging, drug delivery, clean and renewable energy, supercapacitors and batteries, flexible touchscreen displays and ultrafast electronic circuits. [4-11] In order to take most of these applications to a manufacturing level, a low-cost, large scale and simple growth technique for good quality graphene, which meets the efficacy requirement for the respective application, is essential.

To date, there have been numerous approaches for the growth of graphene, such as chemical vapour deposition (CVD) on metal catalysts,[12-13] reduction of graphene oxide (GO),[14] mechanical exfoliation [4] and epitaxial growth on SiC,[15-16] and most of them have inspired many possible future device applications. CVD is a technologically pertinent process as it produces very high quality large-area graphene films, which are transferable to various substrates; however, it is very sensitive to growth conditions such as gas concentration and deposition time[17] and requires the use of relatively complex set-up for the handling of inflammable carbonaceous gases. Other popular methods reported for the production of graphene have their own advantages and limitations. Hence, new, safe and straight-forward methods for the production of good quality graphene are always beneficial.

Physical vapour deposition (PVD) is a scarcely explored technique for the deposition of graphene. There have been a few reports on the use of cathode arc deposition and radio frequency sputtering for the synthesis of FLG.[18-21] However, there appear to be no reports on the utilization of pulsed DC magnetron sputtering (PMS) for the controlled growth of graphene films from single to few layers. PMS technique has developed by combining the benefits of both DC

and RF magnetron sputtering. It has found increasing attention during the past few decades due to its several benefits over RF and DC sputtering including the ability to tune the properties of the film by adjusting the pulse frequency and pulse duty cycle.[22-23] One of the main advantages of PMS is the higher adatom mobility and enhanced surface diffusion,[24] which would be beneficial for improved diffusion of sputtered carbon adatoms to produce better quality graphene films. In addition to that, PMS is cheaper and has a higher deposition rate compared to RF sputtering technology. In this article, we used all the aforementioned benefits of the PMS process for the controlled growth of good quality graphene films with thickness ranging from 3-4 layers to a single layer through a diffusion controlled process. Sputtering is known to be an industrially appropriate manufacturing method for the deposition of large area uniform coatings. Hence, the development of a simple, benign and low-cost graphene growth process based on sputtering would be a significant advancement towards the realization of cheap production of this material. Most importantly, the deposited graphene films by itself show good anticoagulant activity without any pre-treatment or functionalization, which supports the usefulness of the growth process for biomedical applications including the design of blood-contacting medical devices.

## 2. EXPERIMENTAL

### 2.1. Graphene growth on Cu foils

The Cu foil (0.125 mm thick, 99.9%, Goodfellow UK) was pre-treated with acetone, IPA, followed by dipping in to dilute nitric acid (sigma Aldrich) for 2 min and rinsing it using DI water. The cleaned Cu foil is loaded in to the sputtering chamber in which graphite (99.99% pure, Kurt J Lesker) was used as the sputtering target. An ENI RPG-100 pulse generator was used to drive a planar magnetron fitted with the target in the power regulation mode. The chamber was first pumped down to a base pressure of $4.5\times10^{-4}$ mTorr by cryogenic pumping.

The target to substrate distance was adjusted to 9 cm. The power density at the target and duty cycle of the pulse was optimized to be 5.92 W/cm$^2$ and 40%, respectively.

The back side of copper foil was cleaned and the deposited graphene films were then transferred on to glass and $SiO_2$ substrates by removing the Cu using ammonium persulfate etching.

**2.2. Characterization**

Raman spectra were collected at room temperature using a Jobin Yvon Horiba LabRAM 800 spectrometer equipped with an Olympus microscope (objective 100x) and a 488 nm $Ar^+$ laser as the excitation source. Calibration of the spectrometer was performed using a silicon standard with a strong band at 520.07 cm$^{-1}$. The samples were exposed to the laser for 20 s in each scan and the laser spot size was ~ 1 μm. The positions of the peaks were fitted assuming a linear background and a Lorentz peak shape. Graphene films were transferred to Ni TEM grids and HRTEM images were recorded using a JEOL 3000F equipped with an Oxford Instruments. The inter-planar spacing was calculated from HRTEM images using ImageJ software. The transmittance of the graphene film was investigated using a PerkinElmer Lambda 40 UV−vis spectrometer. Morphology of the films was investigated using tapping mode atomic force microscopic (AFM- Veeco Nanoscope Dimension 3100) and scanning electron microscopy (SEM- SEM (Zeiss EVO LS-15) measurements. The x-ray photoelectron spectroscopy (XPS) analysis was carried out using a VG Microtech electron spectrometer at a base pressure of $1\times10^{-9}$ mbar. The photoelectrons were excited with a conventional Mg Kα (hν = 1253.6 eV) x-ray source and an electron energy analyser operating at a 20 eV pass energy, yielding an overall resolution of ~1.2 eV.

**2.3. Anticoagulation studies**

Human fibrinogen (95% clottable and plasminogen depleted) was purchased from Calbiochem (Merck, KGaA, Darmstadt, Germany). Anti-CD41 mouse monoclonal antibody (clone P2, was obtained from Immunotech, Marseilles, France), Alexa Fluor 488 labelled goat anti-mouse was obtained from Invitrogen, (Carlsbad, CA) and 4.5 ml Vacutainer® containing 3.2% sodium citrate were purchased from Becton Dickenson UK Limited, (Oxford, UK). Blood was collected by venepuncture through a 19-gauge needle into a 4.5ml Vacutainer® containing 3.2% (v/v) sodium citrate. The citrated whole blood was used directly in the assay. Whole blood was drawn from healthy, human volunteers who had not taken any medication for at least 10 days before the experiment. 50 µL of fibrinogen solution with a concentration of 200 µg/ml was drop-coated onto a graphene transferred glass slides. The remaining solution from the slide was removed after an hour. The fibrinogen coated slide was then completely blocked with 1 % BSA solution. In whole blood assay, 1 ml of blood was added into the fibrinogen coated glass coverslip and placed in a 35 mm diameter Petri dish. Following blood introduction, the slides were both incubated at 35 oscillations/min for 30 min at room temperature on a "see-saw" rocking platform (Stuart SSL4, Stone, Staffordshire, U.K.). After 30 minutes, the slides were rinsed with PBS buffer and then fixed the platelets with paraformaldehyde (PFA) before labelling. The platelets were labelled using a monoclonal antibody against CD41 and an Alexa-488 fluorescently labelled secondary antibody. Fluorescence images were collected using an Olympus microscope with a 40x objective and the excitation line used was 488 nm. To obtain SEM images of the platelets, fibrinogen- and anti-CD42b antibody-patterned surfaces were incubated with blood, rinsed, and fixed as before. The samples are dehydrated using different concentration of acetone solution as described previously. SEM imaging was performed after gold sputtering on the sample.

## 3. RESULTS AND DISCUSSION

### 3.1. Graphene growth

PMS of a graphite target was carried out in a high purity argon (Ar) (purity-99.999%) atmosphere and the working gas pressure was adjusted to ~4.1 mTorr. The magnetron was pulsed at a frequency of 150 kHz at a 40% duty cycle. The pre-cleaned Cu foil was loaded on to a custom-built heating plate which is heated resistively. The Cu foil was heated to ~700 °C at a higher Ar flow rate (7.5 mTorr) for 5 min to eliminate both surface structural defects and any surface contamination left on the Cu foil even after pre-cleaning and to increase the copper grain size in order to facilitate graphene growth. [25] The temperature was then increased to the growth temperature (varies from 700 °C – 920 °C) and the plasma was ignited to start the sputtering process by powering the target using a pulsed DC supply. The sputtered carbon atoms were deposited on to the heated surface of the Cu foil for 12 min. The plasma was then turned off and the sample temperature was maintained at the growth temperature for a further 3 min. The substrates were then cooled at a rate of ~5.6 °C/s to a temperature of 250 °C and then at a rate of ~0.4 °C/s down to room temperature. The schematic of the experimental set-up and the graphene growth temperature profile is shown in Figures 1 (a) and (b).

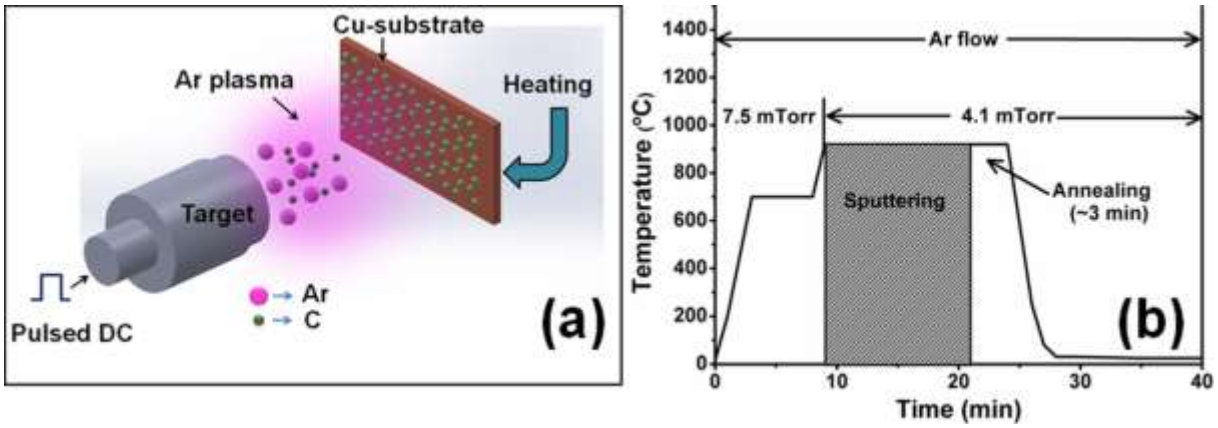

**Figure 1.** (a) Schematic illustration of the experimental set-up used for the growth of graphene films and (b) temperature profile and procedures used for the growth.

Henceforth, the films grown at temperatures of 700 °C, 750 °C, 800 °C, 850 °C and 920 °C are called PSG1, PSG2, PSG3, PSG4 and PSG5.

### 3.2. Structural and optical characterisation of graphene films

Figure 2 shows the AFM height images of pulsed dc sputtered graphene film (PSG) on copper foil deposited at a temperature of 920 °C (PSG5). The figures display the height images of the sample on two different regions of the copper foil; one is a relatively flat (Figures 2(a)) and the other is a sublimation-induced hill and valley formation during graphene growth (Figures 2(b)).[26] Figures 2(c) and 2(d) are the corresponding phase images of figures 2(a) and 2(b). The sublimation induced features were present on a very small portion of the sample, while leaving the rest nearly flat. In addition to that, the sublimation effects were negligible in samples grown at lower temperatures than 920 °C.

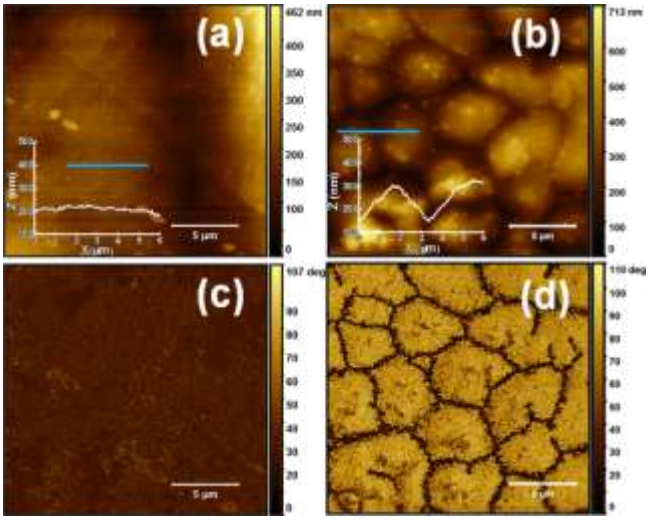

**Figure 2.** AFM images of the graphene film on Cu substrate grown at a temperature of 920 °C. (a) Height images of (a) flat and (b) sublimation-induced hill and valley regions of the sample, respectively. Inset of figures (a) and (b) illustrate the corresponding height profiles along the blue line marked on the images, (c) Phase image of (a) and (d) Phase image of (b). Scale bars are 5 μm in all images.

Recrystallization and grain growth of the underlying copper occurs as the graphene growth temperature is > 900 °C, which is sufficiently larger than the recrystallization temperature of Cu, ~227 °C. [27] The observation of the region as in the hill and valley shapes (Figure 2(a)) is due to the significant sublimation and the loss of copper due to the high temperature.[26] The insets of Figures 2 (a) and (b) show their respective height profiles along the blue horizontal line drawn on the images. The height profiles indicate that the surface observed in Figure 2(a) is more uniform compared to the grainy and hillock features of about 300 nm high and ~ 4 μm widths as seen in Figure 2(b). There are brighter and darker areas corresponding to the higher and lower phase shift manifested on the AFM phase images in Figure 2 (c) and (d). The AFM phase images generally represent the nature of the tip-sample surface interaction and reveal information including hardness, adhesion and elastic modulus. The presence of nanosized features of about 20-200 nm are visible in Figure 2(c), which are believed to be mostly due to the segregation of contaminants from the bulk of the copper sample,[26] however, these features are not easily distinguishable in the height image (Figure 2(a)). Interestingly, Figure 2(d) shows the phase contrast between the grains and grain boundaries, which are not well-resolved and clear in the height image (2(b)). This phase contrast is assumed to be both due to the presence of graphene covered hills with valleys of uncovered copper in between them[26] and non-uniform copper-graphene layer adhesion in the regions where significant copper sublimation occurred.[28]

Optical images of the as received bare copper foil and graphene coated copper foil (PSG5) are indicated in Figures 3(a), (b) and (c) and the corresponding SEM images are presented in Figures 3(d), (e) and (f). The Figures (b) and (e) correspond to the major portion (relatively flat) of PSG5 where sublimation effects were negligible while figures (c) and (f) correspond to the small region (with hillocks) of the sample where significant copper sublimation occurred. The variation of the sublimation rate could be due to either the temperature gradient across the sample or the changes in the crystallographic orientations of copper grains,[26] or a combination of both effects. Optical and SEM images of the bare copper foil heated to 920°C for the same duration (Figures S1 (a) and (b) in the supporting information) do not show the hillock features, which support the view that the growing graphene sheet on the copper surface provides a barrier against sublimation leads to the formation of hillock features.[26]

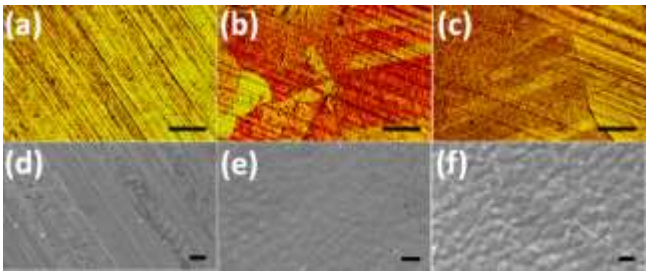


**Figure 3.** Optical and SEM images of bare copper foil (at room temperature) and graphene on copper foil grown at a temperature of 920°C. Optical images of (a) bare copper foil used for the graphene growth and (b-c) graphene coated copper foil regions without (flat) and with (hillocks) considerable copper sublimation. Figures (d), (e) and (f) indicate the corresponding SEM images of figures (a), (b) and (c), respectively. Scale bars in figures (a-c) are 100μm and in figures (d)-(f) are 5μm.

The surface shown in Figure 3(c) appears to be somewhat rougher than that of Figure 3(b) due to the presence of higher hill-valley shapes due to copper sublimation. The SEM image (Figure 3(f)) again reveals the manifestation of mounds of around 3-4 μm width, however, no noticeable hillock formation is observed in the sample region shown in Figure 3(e). SEM images of 2-layer and 3 layer graphene films transferred to and suspended on a TEM grids are indicated in figures S2 (a) and (b) (Supporting information).

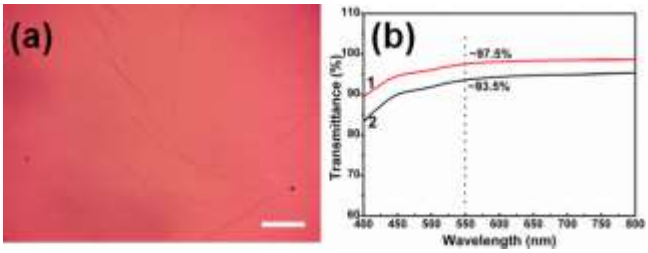


**Figure 4.** Optical image and transmittance of transferred graphene films (a) optical image of graphene film on glass substrate and (b) transmission spectra of graphene films on glass substrate, spectra 1 and 2 represent graphene films with different thicknesses (1-monolayer, 2-~3 layers). Scale bar in figure (a) is 100 μm.

Figure 4(a) shows the optical image of the graphene transferred on to a glass substrate. The formation of wrinkles on the transferred films is visible in the image. Figure 4(b) shows the optical transmission spectra of graphene films transferred onto glass substrates. The two spectra correspond to the transmittance from the graphene films of two different thicknesses. A transmittance of ~97.5% at 550 nm for spectrum 1 corresponds to that of the monolayer graphene (PSG5) and ~93.5% at 550 nm for spectrum 2, which corresponds to 3 layer graphene films (PSG3) as reported in literature.[29-30] The layer numbers of PSG samples have further confirmed using Raman analysis as described in the next section. HRTEM images of the folded

edges of typical graphene samples grown at temperatures 800 and 750 °C are shown in Figures S3 (a) and (b) (supporting information), which reveal the presence of ~2-4 layers of graphene with an inter-planar spacing of ~0.37 nm.[31] Optical and SEM images of a typical graphene film transferred to 90 nm $SiO_2$ coated Si wafer are indicated in Figures S4 (a) and (b), respectively (supporting information).

### 3.3. Raman Spectroscopy

The formation and presence of graphene was detected and characterised using Raman spectroscopy, an essential tool to examine the physical properties of graphene. Figures 5(a) and (b) show the Raman spectra of the films grown on copper foil at various temperatures from 700 °C to 920 °C (samples PSG1- PSG5).

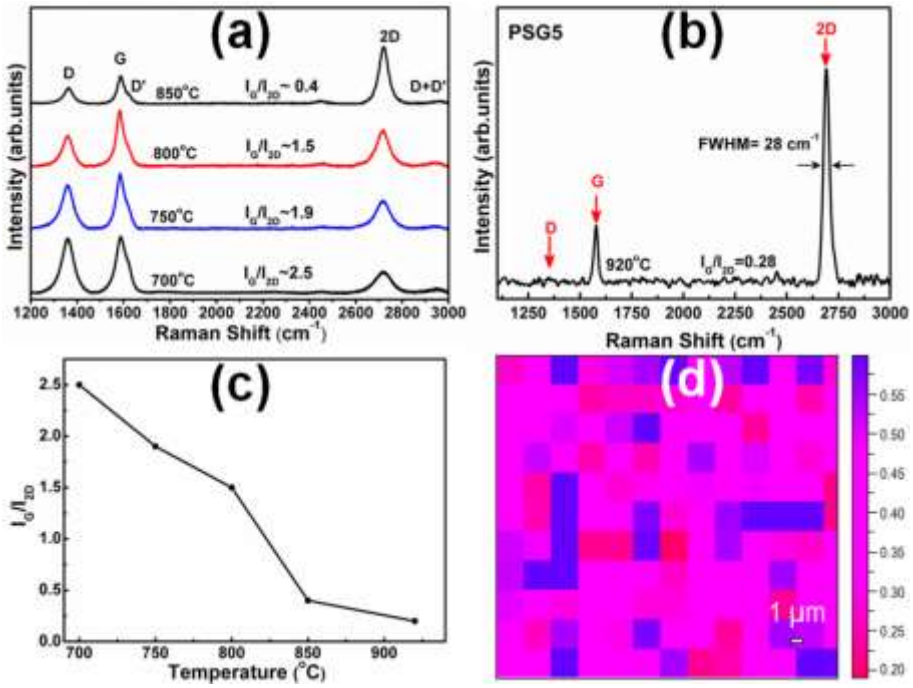


**Figure 5.** (a) Raman spectra of the graphene films at various growth temperatures, (b) Raman spectrum of PSG5 film (grown at 920 °C), (c) Variation of the ratio of the peak intensities $I_G/I_{2D}$

as a function of growth temperature, (d) 2D Raman mapping of the $I_G/I_{2D}$ ratio of graphene on Cu foil (21×25 $\mu m^2$).The laser wavelength used was 488 nm.

The prominent Raman peaks of the PSG5 sample (Figure 5(b)) are the 2D band (second order D peak) at around 2692 $cm^{-1}$ and the G-band (graphite structure) at around 1578 $cm^{-1}$.[30, 32] Figure 5(a) reveals that, as the temperature increases from 700 °C to 920 °C, the intensity of the 2D peak increases while that of the D peak decreases. Figure 5(c) shows the reduction of the intensity ratio of the peaks $I_G/I_{2D}$ from 2.5 (PSG1) to 0.28 (PSG5) as a function of growth temperature from 700 °C to 920 °C, indicating the rise in the degree of graphitization of the film with temperature. Similarly, the decrease in the intensity of the D peak as a function of the growth temperature indicates the enhancement in the quality of the deposited graphene films. The Raman spectrum of the PSG5 film reveals a symmetric 2D peak with a full width at half maximum (FWHM) of ~28 $cm^{-1}$ and a low $I_G/I_{2D}$ value of 0.28, confirming the presence of a monolayer graphene film.[30] In the PSG5 film the D peak is observed only at the noise level suggesting the presence of fewer defects or $sp^3$ carbon atoms,[33] which confirms the good quality of the graphene film comparable with the CVD films.[12] The PSG4 sample equally exhibits a symmetric 2D peak with slightly higher values of FWHM (39 $cm^{-1}$) and $I_G/I_{2D}$ (0.4), which fall within the reported values for monolayer graphene, [34] however, it does display a noticeable D peak (at the edges of graphene) [35]. The D peak represents a breathing mode of $sp^2$ carbon rings and requires a defect or edge for its activation.[36] The D′ band appears close to the G peak at around 1620 $cm^{-1}$ and represents another weak disorder induced peak.[35] The presence of the D peak is expected due to both the lower deposition temperature and the ion bombardment from the plasma during sputtering. The ratio of the D peak to the D′ peak is < 3 in the PSG4 film

indicating mostly boundary-like defects. [37] All the samples studied were post-annealed for 3 min at the growth temperature after the deposition, as explained in the experimental methods. The post-deposition annealing has already been reported to be effective in repairing the plasma created defects in graphene films.[38]

Fig. 5(d) displays a 2-dimentional Raman mapping of the $I_G$ /$I_{2D}$ peak ratio of the PSG5 sample over an area of 21×25 $\mu m^2$. The ratio map indicates that, most of the (> 85%) scanned sample surface is covered with monolayer graphene ($I_G$ /$I_{2D}$ < 0.45) with the remainder consisting of 2 layers [39]. Of particular note is the fact that, using our growth process, most of the sample surface was covered with graphene films composed of either 1-2 layers or more than 2 layers (at 920 °C). Photographs of the floating graphene in ammonium persulfate solution (figure S5) and copper foil surfaces before and after graphene deposition (Figure S6) are shown in the supporting information. We anticipate that further optimization of the sputtering parameters and growth temperature profiles will improve both the domain size and the quality of the deposited graphene films.

### 3.4. Growth mechanism of graphene films

During sputtering, carbon adatoms from the target that are adsorbed on the copper foil, which is heated to the growth temperature (700 - 920 °C), diffuse along the copper surface and start to nucleate when a suitable nucleation site is found. At lower growth temperature *e.g.,* 700 °C, the thermally induced adatom mobility and hence the adatom diffusion rate would be lower. Hence the probability of carbon adatoms to diffusing a sufficient distance to reach the minimum energy sites to nucleate or to make a lattice attachment before they are buried by the subsequent layers would be reduced, and the chance of the perpendicular growth rate increases,[40] forming

multilayer graphene films. In addition to that, at lower temperatures, the adatom desorption rate from the substrate will also be less,[41] which will also contribute towards multilayer formation. As the temperature increases, *e.g.*, >800 °C, the adatom mobility and hence the diffusion rate will be higher thereby increasing the chance of the lateral growth and larger monolayer graphene domain formation. The higher desorption rate of the adatoms at elevated temperature [41] will also reduce the likelihood of multilayer formation. Although the probability of a plasma bombardment created defect would be similar in both higher and lower temperature cases, healing of the defects would be more pronounced at high temperature post-annealing (*e.g.*, at 920 °C).[38] Hence we hypothesise that, since the sputtering time is kept constant, the growth temperature is the important criterion which controls the number of layers and quality of the graphene films. However, at higher temperature values, the likelihood of the copper sublimation also increases and produces copper hillocks underneath the graphene layers, which also affect further diffusion of carbon adatoms, and reduce the size of the graphene islands.

### 3.5. XPS characterisation

Figure 6 shows the curve fitted C 1s curve fitted XPS spectra for the PSG3 and PSG4 samples. There is clear evidence for a prominent asymmetric peak at a binding energy (BE) position of ~284.5 eV which emerges from C=C bonds and is in agreement with the results of Kwon et. al.[42]

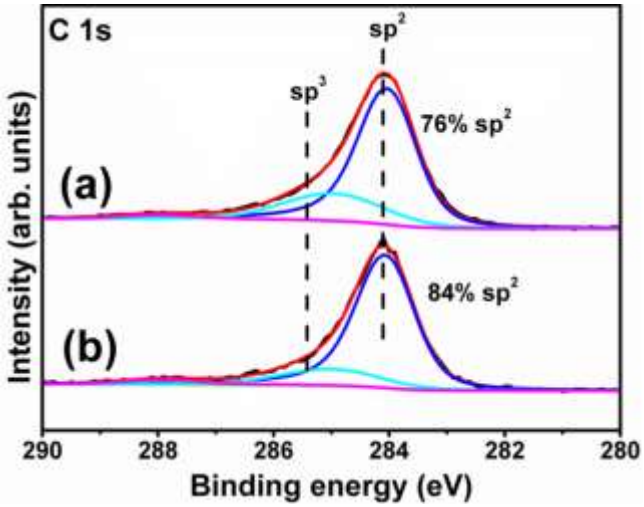


**Figure 6.** XPS C1s spectra from the surface of the graphene grown on copper foil at (a) 800 °C and (b) 850 °C. The prominent peak at 284.5 eV corresponds to $sp^2$ carbon. The pink line exhibits the Shirley background.

The main peak is associated with $sp^2$ carbon, further confirming the formation of graphene. In order to fit the data effectively, an additional symmetric peak is required on the high binding energy side of the $sp^2$ hybridized component peak at a separation of ~1eV. It is suggested that this peak is due to the presence of $sp^3$ hybridized C-C bonds. [42] In order to determine the relative concentrations of the $sp^2$ and $sp^3$ hybridized C 1s components, the integrated areas were calculated. A high proportion of the C 1s peak was determined to be due to the presence of $sp^2$ hybridization with concentrations of 76% and 84% in the PSG3 (800 °C) and PSG4 (850 °C) samples respectively, which again supports the fact that temperature plays key role in determining the quality of the deposited graphene films. A broad peak at around 288 eV represents C=O bond. [42]

### 3.6. Application to anticoagulation

The anticoagulation properties are very important for biomedical application; particularly for blood-contacting surfaces.[43] While using blood-contacting medical devices, one of the most

common issues that lead to complications is the thrombus formation. Hence it is of substantial interest to develop anti-coagulant surfaces to reduce the failure rate of these devices and to minimize the medical complications. Platelet adhesion, activation and aggregation are the major steps in thrombus formation which is mediated by the interaction between receptors in platelets and subendothelial proteins. Platelets play a critical role in hemostasis, a process of stopping bleeding at the site of the interrupted endothelium. Adhesion and activation of the platelets result in the release of chemicals to attract more platelets and triggers a coagulation cascade which then results in the formation of a plug at the site of the injury (thrombus formation). A single step whole blood is used to investigate platelet adhesion, activation and aggregation on the graphene surface.[44]

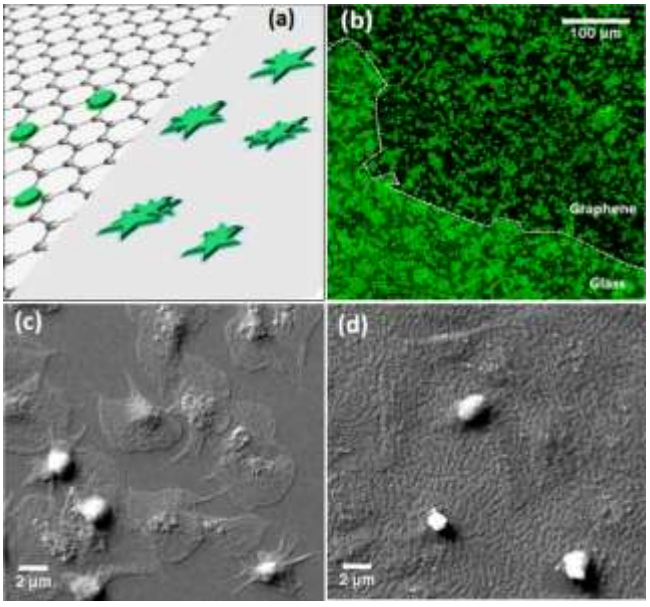


**Figure 7.** (a) Schematic shows captured platelets on fibrinogen coated glass and graphene surfaces (b) Fluorescence microscopic image of platelets captured on fibrinogen coated glass and graphene surfaces. Graphene and bare glass region are indicated on the top and bottom region of the image respectively with the glass-graphene boundary displayed by a white dotted line. SEM images showing the morphology of the platelets captured on the fibrinogen coated (c) glass and (d) graphene surfaces.

Figure 7 (a) shows the schematic of the platelet captured on fibrinogen coated glass and graphene surfaces. Figure 7(b) depicts the fluorescence image of labelled platelets (green colour in the image) on fibrinogen (Fg) coated glass and graphene surfaces. The upper part of image (b) is the graphene covered portion and the lower part is just the bare glass with the glass/graphene boundary indicated as a white dotted line. The image clearly shows a significant reduction in the surface density of the adhered and aggregated platelets in the presence of graphene. Figures 7 (c) and (d) are SEM micrographs of platelets bound to Fg on glass and graphene surfaces respectively. Since platelets change morphology upon activation, SEM images would be an ideal indicator of platelet activation on these surfaces. The presence of fully spread platelets (fried egg like morphology), pseudopodia formation and overlapped structures in figure 7(b) confirms a higher degree of platelet activation and aggregation on Fg/glass surface. [45] The capture of an initial layer of platelets on Fg is observed on for both the graphene and glass regions. However, significant suppression of the adhesion, activation and aggregation of platelets were observed on the Fg/graphene surface (Figure 7 (c)), demonstrated by the presence of spherical platelets free from pseudopodia.

During an injury, initial adhesion of platelets to an external surface results in their full activation including conformational changes in the integrin GPIIb/IIIa receptor on the platelet.[46] GPIIb/IIIa is the most abundant receptor on the surface of a platelet through which fibrinogen binds.[47] Upon activation, platelets release soluble agonists close to the surface which helps to recruit more platelets from flowing blood, and this leads to clot formation. The most important parameter in clot formation is the platelet-platelet interaction through integrin GPIIb/IIIa receptor which happens only after full activation of platelets. Our studies indicated that in the presence of the underlying graphene layer, both the discoid shape of the platelets is maintained

after adhesion to fibrinogen and the platelet-platelet interaction is significantly reduced (Figure 7(d)), indicating the potential anticoagulation activity of the surface. It has been reported that conformation of the adsorbed Fg depends on the surface chemistry of the substrates. [48] Also, platelet adhesion and activation strongly correlates with the adsorption-induced conformational changes in Fg.[49] Another recent report shows that the lack of charge transfer between graphene and Fg inhibits platelet activation on the graphene coated implant samples.[50] Although, the mechanism of the anticoagulation activity of our graphene surfaces is not yet clear, we believe that both the lack of charge transfer and adsorption-induced conformational changes of Fg may have played a significant role. In order to understand the detailed mechanism of the anticoagulation activity, a thorough biological analysis will be required, which is beyond the scope of this article. The excellent anticoagulant activity of the as grown PMS graphene films would be very beneficial for the design of advanced blood contacting materials and medical devices.

## 4. Conclusions

We demonstrate that pulsed DC magnetron sputtering (PMS) is a viable technique for the safe, simple and controlled growth of good quality single and few layer graphene films in pure Ar atmosphere. The PMS approach avails of the higher adatom mobility and surface diffusion, which together with the deposition and post-deposition annealing temperature play significant roles in determining the quality and layer thickness of the formed graphene films. Raman spectral analysis confirms the formation of good quality monolayer graphene at a growth temperature of around 920 °C. The increase of the graphitization of the films as well as the decrease of defect densities was confirmed as a function of the increase of growth temperature. The formation of defect-negligible film at the higher growth temperature is explained by the self-

healing of plasma-induced defects due to the post-deposition annealing. A diffusion mediated growth mechanism is suggested and we have found that the growth temperature is the important criterion which controls the thickness and quality of the graphene films. A simple whole blood assay was performed followed by fluorescence microscopy and SEM analysis to investigate the platelet adhesion, activation and aggregation on the graphene surface. The potential anticoagulant activity of the graphene surface was confirmed by the demonstration of the suppressed adhesion, activation and aggregation of the platelets bound to the Fg/graphene compared to the Fg/Glass surface. We believe that the PMS technique can be easily extended to dope and functionalize graphene with various elements by suitable use of gases or targets during deposition and this would be extremely useful for numerous future applications.

**Conflict of Interest**: The authors declare no competing financial interest.

## ACKNOWLEDGMENTS

We acknowledge the support of Irish Higher Education Authority PRTLI "INSPIRE" project, and Science Foundation Ireland′s Strategic Research Cluster Programme ("Precision" 08/SRC/I1411). KVR acknowledges Dr. Deepak Chandran for his support in graphene transfer and for fruitful discussions. KVR acknowledges B. Roarty and P. Wogan for their technical support.

## SUPPORTING INFORMATION AVAILABLE

Supporting information (Additional SEM, HRTEM, optical and photographs) is available free of charge via the Internet at http://pubs.acs.org.

## References


1. Lee, C.; Wei, X.; Kysar, J. W.; Hone, J., Measurement of the Elastic Properties and Intrinsic Strength of Monolayer Graphene. *Science* **2008,** *321* (5887), 385-388.
2. Novoselov, K. S.; Falko, V. I.; Colombo, L.; Gellert, P. R.; Schwab, M. G.; Kim, K., A Roadmap for Graphene. *Nature* **2012,** *490* (7419), 192-200.
3. Geim, A. K.; Novoselov, K. S., The Rise of Graphene. *Nat Mater* **2007,** *6* (3), 183-191.
4. Novoselov, K. S.; Geim, A. K.; Morozov, S. V.; Jiang, D.; Zhang, Y.; Dubonos, S. V.; Grigorieva, I. V.; Firsov, A. A., Electric Field Effect in Atomically Thin Carbon Films. *Science* **2004,** *306* (5696), 666-669.
5. Lin, Y.-M.; Dimitrakopoulos, C.; Jenkins, K. A.; Farmer, D. B.; Chiu, H.-Y.; Grill, A.; Avouris, P., 100-GHz Transistors from Wafer-Scale Epitaxial Graphene. *Science* **2010,** *327* (5966), 662.
6. Bae, S.; Kim, H.; Lee, Y.; Xu, X.; Park, J.-S.; Zheng, Y.; Balakrishnan, J.; Lei, T.; Ri Kim, H.; Song, Y. I.; Kim, Y.-J.; Kim, K. S.; Ozyilmaz, B.; Ahn, J.-H.; Hong, B. H.; Iijima, S., Roll-to-roll Production of 30-inch Graphene Films for Transparent Electrodes. *Nat. Nanotechnol.* **2010,** *5* (8), 574-578.
7. Xia, F.; Mueller, T.; Lin, Y.-m.; Valdes-Garcia, A.; Avouris, P., Ultrafast Graphene Photodetector. *Nat. Nanotechnol.* **2009,** *4* (12), 839-843.
8. Mazzola, F.; Trinh, T.; Cooil, S.; Østli, E. R.; Høydalsvik, K.; Skjønsfjell, E. T. B.; Kjelstrup, S.; Preobrajenski, A.; Cafolla, A. A.; Evans, D. A.; Breiby, D. W.; Wells, J. W., Graphene Coatings for Chemotherapy: Avoiding Silver-mediated Degradation. *2D Mater.* **2015,** *2* (2), 025004.
9. Tan, X.; Li, Y.; Li, X.; Zhou, S.; Fan, L.; Yang, S., Electrochemical Synthesis of Small-sized Red Fluorescent Graphene Quantum Dots as a Bioimaging Platform. *Chem. Commun.* **2015,** *51* (13), 2544-2546.
10. Kuila, T.; Bose, S.; Khanra, P.; Mishra, A. K.; Kim, N. H.; Lee, J. H., Recent Advances in Graphene-Based Biosensors. *Biosens. Bioelectron.* **2011,** *26* (12), 4637-4648.
11. Huang, L.; Zhang, Z.; Li, Z.; Chen, B.; Ma, X.; Dong, L.; Peng, L.-M., Multifunctional Graphene Sensors for Magnetic and Hydrogen Detection. *ACS Appl. Mater. Interfaces* **2015,** *7* (18), 9581-9588.
12. Li, X.; Cai, W.; An, J.; Kim, S.; Nah, J.; Yang, D.; Piner, R.; Velamakanni, A.; Jung, I.; Tutuc, E.; Banerjee, S. K.; Colombo, L.; Ruoff, R. S., Large-Area Synthesis of High-Quality and Uniform Graphene Films on Copper Foils. *Science* **2009,** *324* (5932), 1312-1314.
13. Chae, S. J.; Güneş, F.; Kim, K. K.; Kim, E. S.; Han, G. H.; Kim, S. M.; Shin, H.-J.; Yoon, S.-M.; Choi, J.-Y.; Park, M. H.; Yang, C. W.; Pribat, D.; Lee, Y. H., Synthesis of Large-Area Graphene Layers on Poly-Nickel Substrate by Chemical Vapor Deposition: Wrinkle Formation. *Adv. Mater.* **2009,** *21* (22), 2328-2333.
14. Bo, Z.; Shuai, X.; Mao, S.; Yang, H.; Qian, J.; Chen, J.; Yan, J.; Cen, K., Green Preparation of Reduced Graphene Oxide for Sensing and Energy Storage Applications. *Sci. Rep.* **2014,** *4*. DOI: 10.1038/srep04684
15. Berger, C.; Song, Z.; Li, X.; Wu, X.; Brown, N.; Naud, C.; Mayou, D.; Li, T.; Hass, J.; Marchenkov, A. N.; Conrad, E. H.; First, P. N.; de Heer, W. A., Electronic Confinement and Coherence in Patterned Epitaxial Graphene. *Science* **2006,** *312* (5777), 1191-1196.

16. Lee, D. S.; Riedl, C.; Krauss, B.; von Klitzing, K.; Starke, U.; Smet, J. H., Raman Spectra of Epitaxial Graphene on SiC and of Epitaxial Graphene Transferred to SiO2. *Nano lett.* **2008,** *8* (12), 4320-4325.
17. Vlassiouk, I.; Regmi, M.; Fulvio, P.; Dai, S.; Datskos, P.; Eres, G.; Smirnov, S., Role of Hydrogen in Chemical Vapor Deposition Growth of Large Single-Crystal Graphene. *ACS Nano* **2011,** *5* (7), 6069-6076.
18. Deng, J.-h.; Zheng, R.-t.; Zhao, Y.; Cheng, G.-a., Vapor–Solid Growth of Few-Layer Graphene Using Radio Frequency Sputtering Deposition and Its Application on Field Emission. *ACS Nano* **2012,** *6* (5), 3727-3733.
19. Ionescu, M. I.; Sun, X.; Luan, B., Multilayer Graphene Synthesized Using Magnetron Sputtering for Planar Supercapacitor Application. *Can. J. Chem* **2014,** *93* (2), 160-164.
20. Oldfield, D. T.; McCulloch, D. G.; Huynh, C. P.; Sears, K.; Hawkins, S. C., Multilayered Graphene Films Prepared at Moderate Temperatures Using Energetic Physical Vapour Deposition. *Carbon* **2015,** *94*, 378-385.
21. Pan, G.; Li, B.; Heath, M.; Horsell, D.; Wears, M. L.; Al Taan, L.; Awan, S., Transfer-free Growth of Graphene on SiO2 Insulator Substrate from Sputtered Carbon and Nickel Films. *Carbon* **2013,** *65*, 349-358.
22. Rajani, K. V.; Daniels, S.; McNally, P. J.; Lucas, F. O.; Alam, M. M., Ultrathin Chromium Transparent Metal Contacts by Pulsed dc Magnetron Sputtering. *Phys. Status Solidi A* **2010,** *207* (7), 1586-1589.
23. Kelly, P. J.; Bradley, J. W., Pulsed Magnetron Sputtering – Process Overview and Applications. *J. Optoelectron. Adv. Mater.* **2009,** *11* (9), 1101-1107.
24. Fateh, N.; Fontalvo, G. A.; Mitterer, C., Structural and Mechanical Properties of dc and Pulsed dc Reactive Magnetron Sputtered V2O5 Films. *J. Phys. D: Appl. Phys.* **2007,** *40* (24), 7716.
25. Mattevi, C.; Kim, H.; Chhowalla, M., A Review of Chemical Vapour Deposition of Graphene on Copper. *J. Mater. Chem.* **2011,** *21* (10), 3324-3334.
26. Wang, Z.-J.; Weinberg, G.; Zhang, Q.; Lunkenbein, T.; Klein-Hoffmann, A.; Kurnatowska, M.; Plodinec, M.; Li, Q.; Chi, L.; Schloegl, R.; Willinger, M.-G., Direct Observation of Graphene Growth and Associated Copper Substrate Dynamics by in Situ Scanning Electron Microscopy. *ACS Nano* **2015,** *9* (2), 1506-1519.
27. Flinn, R. A.; Trojan, P. K., *Engineering Materials And Their Applications: Effect of Stress and Temperature*. Houghton Mifflin Company: Boston, MA, **1981**.
28. Gao, L.; Ni, G.-X.; Liu, Y.; Liu, B.; Castro Neto, A. H.; Loh, K. P., Face-to-face Transfer of Wafer-scale Graphene Films. *Nature* **2014,** *505* (7482), 190-194.
29. Reina, A.; Jia, X.; Ho, J.; Nezich, D.; Son, H.; Bulovic, V.; Dresselhaus, M. S.; Kong, J., Large Area, Few-Layer Graphene Films on Arbitrary Substrates by Chemical Vapor Deposition. *Nano lett.* **2009,** *9* (1), 30-35.
30. Sun, Z.; Yan, Z.; Yao, J.; Beitler, E.; Zhu, Y.; Tour, J. M., Growth of Graphene From Solid Carbon Sources. *Nature* **2010,** *468* (7323), 549-552.
31. Wang, G.; Shen, X.; Yao, J.; Park, J., Graphene Nanosheets for Enhanced Lithium Storage in Lithium Ion Batteries. *Carbon* **2009,** *47* (8), 2049-2053.
32. Calizo, I.; Balandin, A. A.; Bao, W.; Miao, F.; Lau, C. N., Temperature Dependence of the Raman Spectra of Graphene and Graphene Multilayers. *Nano Lett.* **2007,** *7* (9), 2645-2649.

33. Ferrari, A. C.; Meyer, J. C.; Scardaci, V.; Casiraghi, C.; Lazzeri, M.; Mauri, F.; Piscanec, S.; Jiang, D.; Novoselov, K. S.; Roth, S.; Geim, A. K., Raman Spectrum of Graphene and Graphene Layers. *Phys. Rev. Lett.* **2006,** *97* (18), 187401.
34. Ismach, A.; Druzgalski, C.; Penwell, S.; Schwartzberg, A.; Zheng, M.; Javey, A.; Bokor, J.; Zhang, Y., Direct Chemical Vapor Deposition of Graphene on Dielectric Surfaces. *Nano lett.* **2010,** *10* (5), 1542-1548.
35. Malard, L. M.; Pimenta, M. A.; Dresselhaus, G.; Dresselhaus, M. S., Raman Spectroscopy in Graphene. *Phys. Rep.* **2009,** *473* (5–6), 51-87.
36. Casiraghi, C.; Hartschuh, A.; Qian, H.; Piscanec, S.; Georgi, C.; Fasoli, A.; Novoselov, K. S.; Basko, D. M.; Ferrari, A. C., Raman Spectroscopy of Graphene Edges. *Nano Lett.* **2009,** *9* (4), 1433-1441.
37. Eckmann, A.; Felten, A.; Mishchenko, A.; Britnell, L.; Krupke, R.; Novoselov, K. S.; Casiraghi, C., Probing the Nature of Defects in Graphene by Raman Spectroscopy. *Nano lett.* **2012,** *12* (8), 3925-3930.
38. Chen, J.; Shi, T.; Cai, T.; Xu, T.; Sun, L.; Wu, X.; Yu, D., Self Healing of Defected Graphene. *Appl. Phys. Lett.* **2013,** *102* (10), 103107.
39. Levendorf, M. P.; Ruiz-Vargas, C. S.; Garg, S.; Park, J., Transfer-Free Batch Fabrication of Single Layer Graphene Transistors. *Nano lett.* **2009,** *9* (12), 4479-4483.
40. Mahieu, S.; Ghekiere, P.; Depla, D.; De Gryse, R., Biaxial Alignment in Sputter Deposited Thin Films. *Thin Solid Films* **2006,** *515* (4), 1229-1249.
41. Kim, H.; Mattevi, C.; Calvo, M. R.; Oberg, J. C.; Artiglia, L.; Agnoli, S.; Hirjibehedin, C. F.; Chhowalla, M.; Saiz, E., Activation Energy Paths for Graphene Nucleation and Growth on Cu. *ACS Nano* **2012,** *6* (4), 3614-3623.
42. Kwon, K. C.; Ham, J.; Kim, S.; Lee, J.-L.; Kim, S. Y., Eco-friendly Graphene Synthesis on Cu foil Electroplated by Reusing Cu Etchants. *Sci. Rep.* **2014,** *4*. DOI: 10.1038/srep04830
43. Xue, T.; Peng, B.; Xue, M.; Zhong, X.; Chiu, C.-Y.; Yang, S.; Qu, Y.; Ruan, L.; Jiang, S.; Dubin, S.; Kaner, R. B.; Zink, J. I.; Meyerhoff, M. E.; Duan, X.; Huang, Y., Integration of Molecular and Enzymatic Catalysts on Graphene for Biomimetic Generation of Antithrombotic Species. *Nat. Commun.* **2014,** *5*.
44. Basabe-Desmonts, L.; Ramstrom, S.; Meade, G.; O'Neill, S.; Riaz, A.; Lee, L. P.; Ricco, A. J.; Kenny, D., Single-Step Separation of Platelets from Whole Blood Coupled with Digital Quantification by Interfacial Platelet Cytometry (iPC). *Langmuir* **2010,** *26* (18), 14700-14706.
45. Modic, M.; Junkar, I.; Stana-Kleinschek, K.; Kostanjšek, R.; Mozetič, M., Morphology Transformations of Platelets on Plasma Activated Surfaces. *Plasma Processes Polym.* **2014,** *11* (6), 596-605.
46. Coller, B. S., Blockade of Platelet GPIIb/IIIa Receptors as an Antithrombotic Strategy. *Circulation* **1995,** *92* (9), 2373-2380.
47. Hagemeyer, C. E.; Peter, K., Targeting the Platelet Integrin GPIIb/IIIa. *Curr. Pharm. Des.* **2010,** *16* (37), 4119-4133.
48. Marchin, K. L.; Berrie, C. L., Conformational Changes in the Plasma Protein Fibrinogen upon Adsorption to Graphite and Mica Investigated by Atomic Force Microscopy. *Langmuir* **2003,** *19* (23), 9883-9888.
49. Sivaraman, B.; Latour, R. A., The Relationship Between Platelet Adhesion on Surfaces and the Structure Versus the Amount of Adsorbed Fibrinogen. *Biomaterials* **2010,** *31* (5), 832-839.

50. Podila, R.; Moore, T.; Alexis, F.; Rao, A. M., Graphene Coatings for Enhanced Hemocompatibility of Nitinol Stents. *RSC Adv.* **2013,** *3* (6), 1660-1665.

**For Table of Contents Only**